# Scale-free texture of the fast solar wind

B. Hnat,[1] S. C. Chapman,[1] G. Gogoberidze,[1,2] and R. T. Wicks[3]

[1]*Centre for Fusion, Space and Astrophysics, Physics Department, University of Warwick, Coventry, United Kingdom*
[2]*Institute of Theoretical Physics, Ilia State University, 3/5 Cholokashvili Avenue, 0162 Tbilisi, Georgia*
[3]*Space and Atmospheric Group, Physics Department, Imperial College, United Kingdom*

The higher-order statistics of magnetic field magnitude fluctuations in the fast quiet solar wind are quantified systematically, scale by scale. We find a single global non-Gaussian scale-free behavior from minutes to over 5 h. This spans the signature of an inertial range of magnetohydrodynamic turbulence and a $\sim 1/f$ range in magnetic field components. This global scaling in field magnitude fluctuations is an intrinsic component of the underlying texture of the solar wind and puts a strong constraint on any theory of solar corona and the heliosphere. Intriguingly, the magnetic field and velocity components show scale-dependent dynamic alignment outside of the inertial range.

*In situ* spacecraft observations of plasma parameters in the interplanetary high Reynolds number solar wind flow [1] provide time series over several decades that are ideally suited to studies of turbulence and of other phenomena that generate statistical scaling. These observations show a power-law range of power spectral density (PSD) in magnetic field and velocity components which is associated with an inertial range of magnetohydrodynamic (MHD) turbulence (see, e.g., Ref. [2]). This inertial range phenomenology is seen from ion kinetic scales up to an outer scale at which there is a crossover to a $\sim 1/f$ power-law range of the PSD in the field components of coronal origin [1,3].

There is debate as to which aspects of these observations should be attributed to MHD turbulence. The dominant velocity and magnetic field components fluctuations are found in the inertial range of scales and these *do* exhibit statistical signatures consistent with evolving MHD turbulence: intermittency [4], non-Gaussian statistics [5], and anisotropy [6,7]. This inertial range extends to lower frequencies both with increasing solar distance and in slow as compared to fast solar wind, suggesting an actively evolving turbulent cascade [8,9]. However, such a cascade evolves in the presence of fluctuations of coronal origin, the "texture" of the solar wind [10,11]. This nontrivial texture, in the absence of turbulence, can be inferred, at least on longer scales, from the observed $\sim 1/f$ fluctuations in the magnetic field components. These show latitudinal variation and statistical scaling distinct from that of the inertial range [1,12,13].

Since the earliest *in situ* observations [14] the relative importance of turbulence in these signatures has been debated. Recently, it has been argued that the range of PSD scaling exponents routinely measured in the inertial range for magnetic field components can arise from a nonevolving set of discontinuities [15]. However, distinct physical mechanisms can share the same power-law exponent in the PSD [16]. In the context of Alfvénic MHD turbulence in the solar wind, where discussion naturally centers on the components of velocity and magnetic field, such discontinuities can arise from turbulence or be part of the solar wind texture. To the best of our knowledge, there is no unique procedure to distinguish these two physical signatures. To understand the texture of the solar wind it is

thus informative to consider scalar parameters alongside vector components.

Intriguingly, in the solar wind, scalar plasma parameters such as magnetic field magnitude $|\mathbf{B}|$, energy density $B^2$, and density $n$ show scaling, and this is also a feature of the texture of the solar wind. A power-law range in the PSD of $|\mathbf{B}|$ is seen to extend through the inertial range into the $\sim 1/f$ range of frequencies but at 1 Astronomical Units (A.U.) is typically a decade lower in power compared to that of the magnetic field components $B_k$ [17]. Scalar magnetic field and plasma parameters can also show scaling in long-time bulk hourly averages [18] and aggregate statistics up to tens of hours [19,20]. Pioneering work with HELIOS [21–23] showed that $|\mathbf{B}|$ power spectral exponent is roughly invariant with radial distance at frequencies below $10^{-2}$ Hz; a "flattening" at higher frequencies seen in the inner heliosphere is not seen at 1 Astronomical Units (A.U.) (however, our analysis will not approach these high frequencies). There is an admixture of compressive fluctuations and pressure balanced structures [24,25]; $|\mathbf{B}|$ and $n$ do not simply advect together as passive scalars [26].

Distinct physical mechanisms that generate scaling can share the same power-law exponent in the PSD [27] and thus statistical scaling of the higher-order moments is an essential tool needed to distinguish them. In this Rapid Communication we perform a systematic scale-by-scale study of the statistical scaling properties of $|\mathbf{B}|$ fluctuations in extended intervals of fast, quiet solar wind. We find global scale-free behavior in $|\mathbf{B}|$ fluctuations which occurs alongside, but is quite distinct from, that of the components of magnetic field, and extends through both the inertial and $\sim 1/f$ ranges of temporal scales. Thus we establish scaling is an intrinsic feature of the texture of the solar wind operating through the inertial and $\sim 1/f$ ranges. This suggests that a single stochastic process for magnetic field magnitude fluctuations is operating or has operated across this full range of MHD time scales supported by the solar wind.

A corollary of this result is that it provides a natural laboratory to test proposed measures of *in situ* MHD turbulence, since within the same dataset fluctuations may be generated by turbulence (the inertial range) and on longer scales may be of solar origin. Scaling exponents predicted

by theories of turbulence are difficult to determine accurately in data [28,29], hence the attraction to test signatures such as scale-dependent dynamic alignment [30]. Direct numerical simulations (DNSs) [31,32] have suggested such alignment [33], in which turbulent fluctuations of velocity and magnetic field progressively align in the cascade, to be a signature of anisotropic MHD turbulence. This has recently attracted controversy [34,35], which we will address directly from the observations.

We use *in situ* observations of fast solar wind from the ACE and Ulysses spacecraft [36]. ACE is at ∼1 Astronomical Units (A.U.) in the ecliptic, whereas for the intervals under study, Ulysses was at a heliospheric latitude above 70° at ∼2.2 Astronomical Units (A.U.); thus we can compare solar wind of distinct coronal origin. We selected continuous intervals of quiet fast solar wind flow at solar minimum which did not contain large coherent structures or large-scale, long-time secular change in the ion plasma pressure (estimated as $nT$). Fast wind intervals have been identified using the following criteria: $\langle v_{sw} \rangle \geqslant 550$ km/s and its standard deviation $\sigma(v_{sw}) \leqslant 50$ km/s, where $v_{sw}$ is the speed of the solar wind. Five stationary fast solar wind intervals were identified in ACE 2007 and 2008 datasets of 64-s average calibrated magnetic field magnitude and plasma observations. The Ulysses observations correspond to five intervals of 3 days duration (July 1–17) of the 1995 (solar minimum) north polar pass. We used 1-min average calibrated magnetic field data for the magnetic field analysis only. Ulysses plasma 4-min averaged observations were combined with magnetic field data by selecting the 1-s cadence magnetic field records that match plasma observations times to the nearest second.

All statistical measures are first computed individually for each interval; these are cubic spline interpolated onto a common temporal or frequency grid and then an average over all five intervals for each of ACE and Ulysses is obtained. The longest time scale is fixed by that of the shortest data interval so that we can access time scales over the range ∼2 min to ∼20 h. Practically, given the effect of averaging onto 64 s and nonuniformities in the time base, we do not draw strong conclusions from analysis on time scales shorter than ∼3 min. We will indicate with error bars on our plots the rms variation about the sample average across the intervals. The averaged, smoothed PSD (Welch modified periodogram) of the magnetic field magnitude for both ACE and Ulysses intervals is shown in Fig. 1 alongside that of one of the components: $B_x$ (ACE) and $B_R$ (Ulysses). These curves have been displaced vertically in the figure for clarity. Typically, the magnetic field components are a factor of 5 higher in power compared to |**B**| for these intervals and on this plot show a steeper power-law trend at higher frequencies with exponent $s$ close to the often observed $\approx \frac{5}{3}$ "inertial range" value. Figure 1 shows that at a time scale 20–30 min the components depart from $\approx \frac{5}{3}$ inertial range scaling and crossover to a ∼$1/f$ spectrum. This time scale is indicated on all subsequent plots. The PSD of |**B**| follows a single power law over the entire range with exponent $\approx -1.4$, a behavior that is distinct from that of the components. The Ulysses and ACE observations show essentially the same behavior in the PSD: a transition from inertial range to ∼$1/f$ scaling in the components (also seen in the other components, not shown) and alongside this, a single range of scaling in the
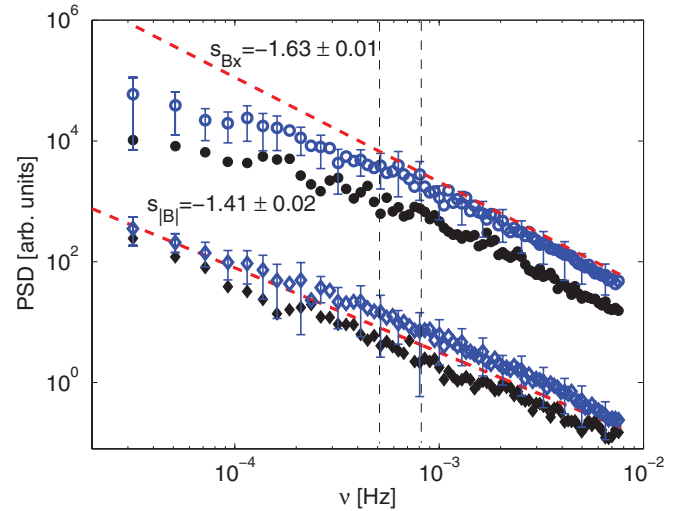


FIG. 1. (Color online) Averaged PSD of magnetic field GSE component $B_x$ from ACE (solid circle, black), RTN component $B_R$ from Ulysses (open circle, blue), and magnetic field magnitude: ACE, filled diamond (black); Ulysses, open diamond (blue). PSDs were displaced vertically for clarity; dashed lines indicate time scales of 20 and 30 min.

magnitude with an exponent distinct from that of the inertial range. We now consider the statistical scaling in the higher moments of the fluctuations. On a given temporal scale $\tau$, the fluctuations are $\delta x(t,\tau) = x(t + \tau) - x(t)$ in the time series of a given (scalar or vector) quantity $x(t)$. In Fig. 2 we plot, for the same quantities shown in Fig. 1, the kurtosis of the fluctuations $K = \mu_4/\mu_2^2$, where $\mu_k = \langle (\delta x(t,\tau) - \langle \delta x(t,\tau) \rangle)^k \rangle$ are their central moments. For a Gaussian probability density function (PDF), $K = 3$, and this is indicated with a dashed horizontal line. The components (within variance of the average) show a smooth and scale-free drop in kurtosis within the inertial range, on scales shorter than ∼20–30 min. At ∼20–30 min
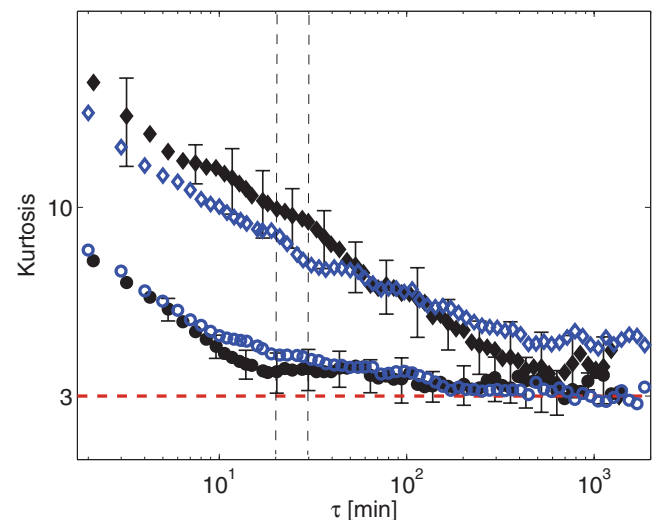


FIG. 2. (Color online) Kurtosis of magnetic field component $B_x$ from ACE (solid circle, black), component $B_R$ from Ulysses (open circle, blue), and magnetic field magnitude: ACE, solid diamond (black); Ulysses, open diamond (blue).

there is a "kink" at the end if the inertial range, beyond which the PDFs are weakly non-Gaussian ($K > 3$) and progressively approach Gaussian at scales $\sim$120 min. The behavior of $\delta|\mathbf{B}|$ is clearly distinct from that of the components, and is far from Gaussian until much longer time scales, beyond $\sim$5 h [37]. On scales shorter than $\sim$5 h the behavior in the kurtosis seen in fast quiet solar wind streams in the ecliptic (ACE) roughly tracks that seen in polar outflows (Ulysses); fluctuations of $|\mathbf{B}|$ are not sensitive to the distinct coronal origin of these flows until the longest temporal scales are reached. We note that, in principle, more information can be obtained from signed structure functions of odd moments, however, consistent with Refs. [38] and [39], we find that these signed quantities do not produce homogeneous results across all intervals studied here, therefore, it is not appropriate to average these.

Figures 1 and 2 together establish a quite remarkable result: There is a single scale-free behavior in fluctuations of $|\mathbf{B}|$ spanning three decades in temporal scales from $\sim$2 min to over 5 h. The scale-free signatures extend through both the inertial and $\sim$1/$f$ ranges of temporal scales seen in these same intervals in the field components. This suggests a physical mechanism for $|\mathbf{B}|$ scaling across all these scales that is distinct from the *in situ* Aflvénic MHD turbulence that is driving scaling in the components. Compressive fluctuations and pressure balanced structures [25] are natural candidates for magnetic field magnitude fluctuations—they can in principle be dynamically evolving or passively advecting, having been generated in the formation of the solar wind. In Fig. 3 we directly compare the PSD of $|\mathbf{B}|$ from ACE and Ulysses as shown in Fig. 1 with that of the density. The scaling of the density closely follows that of $|\mathbf{B}|$ in the $\sim$1/$f$ range, but departs on time scales shorter than 20–30 min, that is, where the inertial range is seen in the magnetic field components. In the inertial range, the power in the density fluctuations is enhanced above that which would arise from the scaling seen on longer time scales. Essentially the same behavior is seen in both ACE and Ulysses and thus again is not strongly sensitive to the region of coronal origin. However, caution is needed when interpreting density fluctuations at the smallest scales, due to uncertainty that may affect the measurements [40]. Given this caveat, the single range of scaling in $|\mathbf{B}|$ fluctuations that extends through both the inertial and $\sim$1/$f$ ranges of scale thus does not straightforwardly correspond to the behavior of the density fluctuations. Thus one cannot invoke a single process to generate the scaling of fluctuations in both $|\mathbf{B}|$ and density unless some process operating in the inertial range acts to enhance density fluctuations.

Finally, we will look more closely at the behavior of the components of fluctuations across both the inertial and $\sim$1/$f$ ranges of scale. We explore this idea by performing a dynamic alignment analysis across the full range of scales available in our chosen intervals. Dynamic alignment, calculated scale by scale as the relative angle between the vector fluctuations $\delta\mathbf{v}_\perp$ and $\delta\mathbf{b}_\perp$ [30,33], has been proposed as a signature of the turbulent cascade [33]. Perpendicular directions are taken with respect to the mean local magnetic field, which at time $t$ is given by an average $\langle\mathbf{B}(t)\rangle$ computed over a scale-dependent interval $[t - \tau, t + \tau]$. Perpendicular fluctuations are then obtained from the following expressions: $\delta\mathbf{v}_\perp = \delta\mathbf{v} - (\delta\mathbf{v} \cdot \hat{\mathbf{b}})\hat{\mathbf{b}}$ and $\delta\mathbf{b}_\perp = \delta\mathbf{b} - (\delta\mathbf{b} \cdot \hat{\mathbf{b}})\hat{\mathbf{b}}$, where the unit vector $\hat{\mathbf{b}} = \delta\mathbf{B}/B$. The average angle of alignment is

$$\Theta(\tau) = \arcsin\left(\frac{\langle|\delta\mathbf{v}_\perp \wedge \delta\mathbf{b}_\perp|\rangle}{\langle\delta v_\perp\rangle\langle\delta b_\perp\rangle}\right). \tag{1}$$

In Fig. 4 we plot this average angle $\Theta(\tau)$ as a function of scale $\tau$ for the same intervals shown in Figs. 1–3. On such a plot, progressively aligning field and flow fluctuations should show a scale-free decrease in $\langle\Theta\rangle$ with decreasing scale $\tau$ within the inertial range; as the cascade progresses from large to small scales the field and flow progressively align [33]. However, Fig. 4 show this behavior most strongly on temporal scales $\tau > 100$ min, well into the $\sim$1/$f$ range of scales. Indeed, the variation of $\langle\Theta\rangle$ with increasing scale $\tau$ asymptotes to within errors of that predicted for *in situ* turbulence [33]. Thus "dynamic alignment," as quantified by (1), is not a clear discriminator of turbulence in the solar wind, but intriguingly,
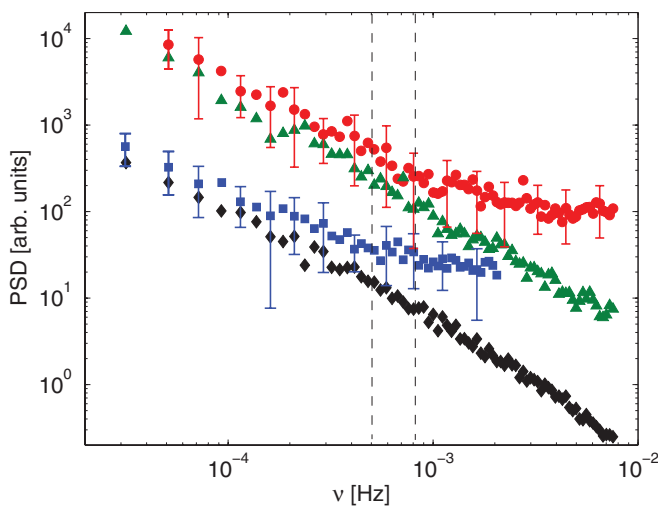


FIG. 3. (Color online) Average PSD of magnetic field magnitude [ACE, triangle (green); Ulysses, diamond (black)] and density [ACE, circle (red); Ulysses, square (blue)].
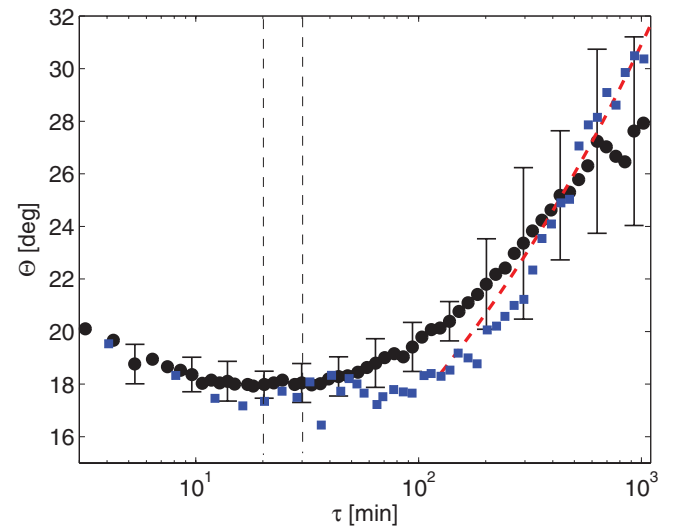


FIG. 4. (Color online) Average angle of perpendicular fluctuations in velocity and magnetic field: ACE, circle (black); Ulysses, square (blue). An asymptote of $\Theta \sim \tau^{0.25}$ is indicated on the plot.

in the absence of *in situ* MHD turbulence, that is, in the $\sim 1/f$ range it is coincident with scaling in fluctuations of $|\mathbf{B}|$.

We have established that there is a scale-free behavior in $|\mathbf{B}|$ fluctuations that occurs alongside, but is quite distinct from, that of the components of magnetic field. It extends over three decades through both the inertial and $\sim 1/f$ ranges of temporal scales and is seen in fast quiet solar wind of different coronal origin. The most parsimonious description of how such a single scaling range in $|\mathbf{B}|$ could arise is that a single process operates, or has operated, over all these scales. Observational evidence of incompressible MHD turbulence in the solar wind must thus be understood in the context of the global *scaling* of the "texture" [10,11] of the solar wind. We have also shown that scale-dependent "dynamic alignment" is not a clear discriminator of turbulence in the solar wind. This "pseudo-dynamic alignment," taken alongside the scaling seen in the magnitude of magnetic field, may, however, provide an insight into the generation of the flux tube texture of the solar wind. It may capture some physics of the generation of the solar wind, reflecting the manner in which magnetic helicity is injected via photospheric fields that are fractal [41].

[1] W. H. Matthaeus *et al.*, Astrophys. J. **657**, L121 (2007).

[2] M. L. Goldstein, D. A. Roberts, and W. H. Matthaeus, Annu. Rev. Astron. Astrophys. **33**, 283 (1995).

[3] W. H. Matthaeus and M. L. Goldstein, Phys. Rev. Lett. **57**, 495 (1986).

[4] T. S. Horbury and A. Balogh, Nonlin. Proc. Geophys. **4**, 185 (1997).

[5] E. Marsch and C.-Y. Tu, Nonlin. Proc. Geophys. **4**, 101 (1997).

[6] L. J. Milano, S. Dasso, W. H. Matthaeus, and C. W. Smith, Phys. Rev. Lett. **93**, 155005 (2004).

[7] S. C. Chapman and B. Hnat, Geophys. Res. Lett. **34**, L17103 (2007).

[8] T. S. Horbury, A. Balogh, R. J. Forsyth, and E. J. Smith, Astron. Astrophys. **316**, 333 (1996).

[9] E. Marsch and C.-Y. Tu, J. Geophys. Res. **101**, 11149 (1996).

[10] R. Bruno *et al.*, Ann. Geophys. **25**, 1913 (2007).

[11] J. E. Borovsky, J. Geophys. Res. **113**, A08110 (2008).

[12] R. M. Nicol, S. C. Chapman, and R. O. Dendy, Astrophys. J. **679**, 862 (2008).

[13] S. C. Chapman and R. M. Nicol, Phys. Rev. Lett. **103**, 241101 (2009).

[14] P. J. Coleman, Astrophys. J. **153**, 371 (1968).

[15] J. E. Borovsky, Phys. Rev. Lett. **105**, 111102 (2010).

[16] S. C. Chapman, B. Hnat, and K. Kiyani, Nonlin. Proc. Geophys. **15**, 445 (2008).

[17] M. L. Goldstein and D. A. Roberts, Phys. Plasmas **6**, 4154 (1999).

[18] L. Burlaga, J. Geophys. Res. **97**, 4283 (1992).

[19] B. Hnat *et al.*, Geophys. Res. Lett. **29**, L86 (2002).

[20] K. Kiyani, S. C. Chapman, B. Hnat, and R. M. Nicol, Phys. Rev. Lett. **98**, 211101 (2007).

[21] K. U. Denskat and F. M. Neubauer, J. Geophys. Res. **87**, 2215 (1982).

[22] B. Bavassano *et al.*, J. Geophys. Res. **87**, 3617 (1982).

[23] E. Marsch and C.-Y. Tu, J. Geophys. Res. **95**, 11945 (1990).

[24] P. J. Kellog and T. S. Horbury, Ann. Geophys. **23**, 3765 (2005).

[25] C.-Y. Tu and E. Marsch, J. Geophys. Res. **99**, 21481 (1994).

[26] B. Hnat, S. C. Chapman, and G. Rowlands, Phys. Rev. Lett. **94**, 204502 (2005).

[27] D. Sornette, *Critical Phenomena in Natural Sciences; Chaos, Fractals, Self-organization and Disorder: Concepts and Tools* (Springer, Berlin, 2000).

[28] T. Dudok de Wit, Phys. Rev. E **70**, 055302 (2004).

[29] K. H. Kiyani, S. C. Chapman, and N. W. Watkins, Phys. Rev. E **79**, 036109 (2009).

[30] J. J. Podesta *et al.*, J. Geophys. Res. **114**, A01107 (2009).

[31] W.-C. Müller, D. Biskamp, and R. Grappin, Phys. Rev. E **67**, 066302 (2003).

[32] A. Beresnyak and A. Lazarin, Astrophys. J. **640**, L175 (2006).

[33] S. Boldyrev, Phys. Rev. Lett. **96**, 115002 (2006).

[34] A. Beresnyak and A. Lazarian, Astrophys. J. **702**, 1190 (2009).

[35] A. Beresnyak, Phys. Rev. Lett. **106**, 075001 (2011).

[36] Data obtained from the CDAWeb site http://cdaweb.gsfc.nasa.gov/.

[37] R. Bruno *et al.*, J. Geophys. Res. **108**, 1130 (2003).

[38] V. Carbone, R. Marino, L. Sorriso-Valvo, A. Noullez, and R. Bruno, Phys. Rev. Lett. **103**, 061102 (2009).

[39] L. Sorriso-Valvo, V. Carbone, R. Marino, A. Noullez, R. Bruno, and P. Veltri, Phys. Rev. Lett. **104**, 189002 (2010).

[40] D. J. McComas *et al.*, Geophys. Res. Lett. **25**, 4289 (1998).

[41] K. Jansen, A. Vogler, and F. Kneer, Astron. Astrophys. **409**, 1127 (2003).